# Thin mixed matrix and dual layer membranes containing metal-organic framework nanosheets and Polyactive™ for $CO_2$ capture

Sabetghadam, Anahid; Liu, Xinlei; Gottmer, Soraya; Chu, Liangyong; Gascon, Jorge; Kapteijn, Freek

**DOI**
10.1016/j.memsci.2018.10.047

**Publication date**
2019

**Document Version**
Final published version

**Published in**
Journal of Membrane Science

Journal of Membrane Science 570–571 (2019) 226–235

Contents lists available at ScienceDirect

Journal of Membrane Science

journal homepage: www.elsevier.com/locate/memsci

# Thin mixed matrix and dual layer membranes containing metal-organic framework nanosheets and Polyactive™ for $CO_2$ capture

Anahid Sabetghadam[a], Xinlei Liu[a], Soraya Gottmer[a], Liangyong Chu[b], Jorge Gascon[a,c], Freek Kapteijn[a]

[a] Catalysis Engineering, Department of Chemical Engineering, Delft University of Technology, Van der Maasweg 9, 2629HZ Delft, The Netherlands
[b] Organic Materials and Interfaces, Department of Chemical Engineering, Delft University of Technology, Van der Maasweg 9, 2629HZ Delft, The Netherlands
[c] KAUST Catalysis Center, King Abdullah University of Science and Technology, Advanced Catalytic Materials, Thuwal 23955, Saudi Arabia

ARTICLE INFO

*Keywords:*
MOF nanosheets
Polyactive™
Cu-BDC
Mixed matrix membranes
Dual layer
Gas separation
$CO_2/N_2$

ABSTRACT

Preparation methods are presented of thin dual layer membranes (DLM's) and mixed matrix membranes (MMM's) based on nanosheets of the Cu-BDC metal-organic framework (MOF, lateral size range 1–5 μm, thickness 15 nm) and commercially available poly(ethylene oxide)–poly(butylene terephthalate) (PEO–PBT) copolymer (Polyactive™) and their performances are compared in $CO_2/N_2$ separation. The MMMs and DLMs represent two extremes, on the one hand with well-mixed components and on the other hand completely segregated layers. Compared to the free-standing membranes, the thin PAN- and zirconia-alumina-supported MMMs showed significant enhancement in both permeance and selectivity. The support properties affect the obtained selective layer thickness and its resistance impacts the $CO_2/N_2$ selectivity. The permeance of thin DLM's is among the highest reported literature data of MOF based thin MMMs, but have a modest selectivity. Addition of the nanosheets in the thin MMMs improves the $CO_2/N_2$ selectivity of the already selective polymer further to 77. The nanosheets in the thin MMMs make a gutter layer on the PAN support superfluous. The small pore support $ZrO_2$-alumina does not need a gutter layer.

XRD analysis reveals that the spatial distribution of MOF nanosheets and polymer chains packing were responsible for differences in the permeation performance of the free-standing, thin dual layer and mixed matrix membranes.

## 1. Introduction

The increasing global demand for energy-efficient separations in carbon capture has prompted international actions on searching for novel, high-performance separation membranes [1]. For industrial scale applications such as natural gas sweetening [2], $CO_2$ capture from flue gas [3] and $H_2$ separation from syngas [4], the use of highly permeable and selective membranes is essential. Industrial-scale gas separation applications require production of large membrane areas (e.g., $10^5$ to $10^7$ $m^2$) with low defect densities (e.g., below 1 $m^2$ per $10^5$ $m^2$ of membrane surface area) [5]. Such a scale-up is often quite challenging and requires the production of thin, defect free membranes using industrial membrane fabrication methods [6]. Membranes with very thin selective layers (asymmetric or composite structure) typically in the range of 0.1–2 μm are required. The first thin asymmetric membrane was made by phase inversion and reported by Loeb-Surirajan in 1959. The asymmetric structure consisted of a 0.2–0.5 μm thin skin layer supported by a porous substructure with 0.1–1.0 μm pore size [7]. Another class of thin membranes can be prepared by coating a thin selective layer on a porous support which are known as thin supported membranes [8]. These membranes are cheaper to manufacture on industrial scale due to the lower consumption of material for the selective layer preparation and the use of commercial porous supports. The most widely used methods for preparing thin supported membranes are drop-casting [9], dip-coating [10] and spin coating [11].

Commonly, thin membranes may also have an intermediate layer known as gutter layer between the porous support and the selective layer. The gutter layer is mainly chosen from highly permeable polymers such as PDMS [9] or PTMSP [12] to afford a smooth and flat coating surface while preventing the upper selective layer penetration into the support. This method also heals defects in the support layer improving the membrane quality, constituted a breakthrough in the application of polymeric membranes [13,14].

Regarding greenhouse gas emission reduction $CO_2$ selective membranes are subject of many studies. Membranes with $CO_2/N_2$ selectivities > 30 and high permeances are required in post-combustion $CO_2$

*E-mail addresses:* a.sabetghadamesfahani@tudelft.nl (A. Sabetghadam), f.kapteijn@tudelft.nl (F. Kapteijn).

https://doi.org/10.1016/j.memsci.2018.10.047
Received 9 September 2018; Received in revised form 9 October 2018; Accepted 17 October 2018
Available online 19 October 2018
0376-7388/ 

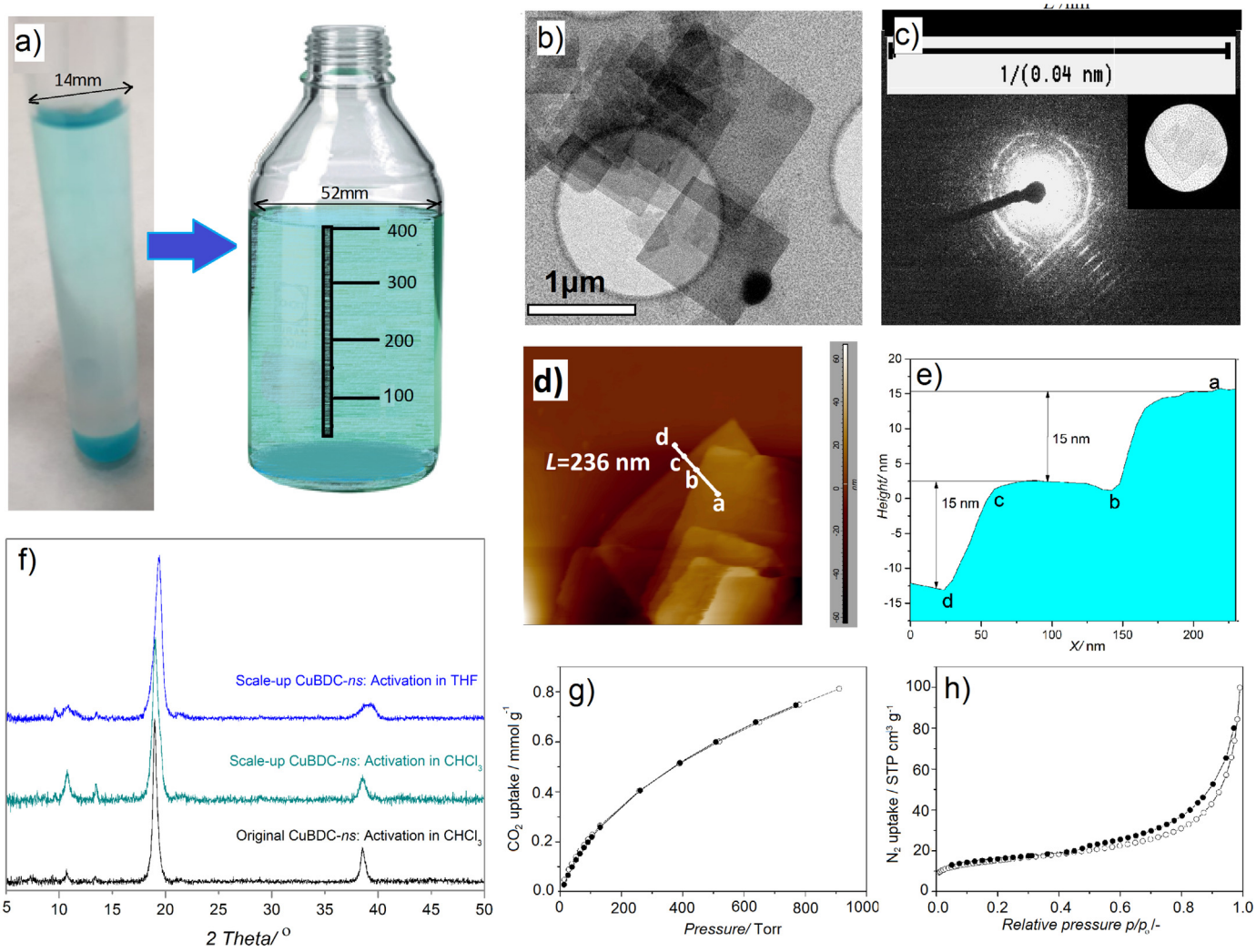


**Fig. 1.** Cu-BDC nanosheet original and scaled-up synthesis (a), TEM images and electron diffraction pattern of region shown in inset (b, c), AFM image showing the thickness of Cu-BDC nanosheets (d, e), XRD patterns of original [39] and scaled-up synthesis using chloroform or THF washing (f), $CO_2$ and $N_2$ adsorption of Cu-BDC nanosheets at 273 and 77 K (g, h) (the open and closed symbols represent the adsorption and desorption data, respectively.

capture to reduce the energetic impact [15,16]. Glassy-rubbery polymers like Pebax and Polyactive™ types with selectivities around 50 are most studied. The Polaris membrane belonging to these materials [17] has shown excellent permeances as well [14]. The question arises if the separation performance of such polymeric membranes can be improved even further. High selectivities may reduce the required membrane area or even change the process lay-out [13]. A feasible approach to improve the selectivity is the incorporation of fillers (e.g., micro- or nanoparticles) in the polymeric matrix to form mixed matrix membranes (MMMs) [18]. However, thin MMMs potentially suffer from defect formation during the fabrication process due to a poor compatibility between filler and matrix, which makes their large-scale production quite challenging. One strategy to prepare defect free ultra-thin mixed matrix membranes is using polymers that address the compatibility and ageing issues. Glassy-rubbery block copolymers such as Pebax® have been widely studied to make the defect-free MMMs due to their low glass transition temperature and chain flexibility, filling the gaps between filler and polymer.[19–21] Using Pebax® 1657 as the continuous matrix resulted in MMMs featuring moderate $CO_2$ permeability and relatively high selectivity over $N_2$ and $CH_4$, making it an attractive polymer for defect free thin membrane formation [10,22–26]. Polyactive™, composed of poly(ethylene oxide) (PEO) and poly(butylenes terephthalate) (PBT) segments, is another promising block copolymer for $CO_2$ separation which has been fabricated as thin membrane and used in pilot scale modules [27]. To fabricate defect-free thin membranes the use of high molecular weight polymer was needed [28].

Considering the compatibility issues in mixed matrix membranes, metal-organic frameworks are known as potential candidate with improved polymer-filler interaction. This is mainly ascribed to the organic linker functional groups that can interact with the polymer chains [29,30].

Another approach to address difficulties in fabricating large-scale, defect-free thin MMMs is the use of nanomaterials with a high aspect ratio (e.g., carbon nanotubes [31], graphene [32], 2D zeolites [33] and MOF nanosheets [34]) as fillers [35,36]. In this regard MOFs offer a number of advantages, since their morphology can be tuned in a relatively straightforward manner. As example, different morphologies of $NH_2$-MIL-53(Al) such as nanorod, microneedle, nanoparticle and nanosheet were synthesized via using various synthetic approaches [37,38]. Cu-BDC bulk and nanosheet morphologies were compared by Rodenas *et al.* [39] and even the preparation of non-lamellar MOF nanosheets has recently been reported [38]. In general, two different synthesis routes have been reported for 2D MOF materials, which are globally (*i*) top-down and (*ii*) bottom-up synthesis approaches. The first approach relies on exfoliation of 3D materials that have some drawbacks such as crystal or morphological damage and re-aggregation of the exfoliated material [40,41]. The second approach is preferably used in synthesis of ultra-thin sheets in which the aspect-ratio is possible to

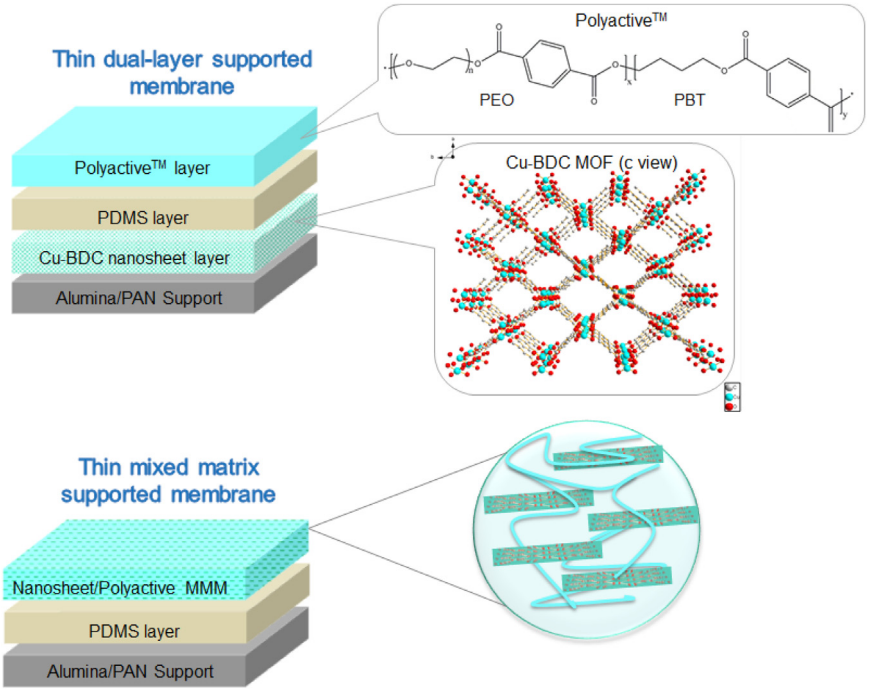


**Fig. 2.** Scheme of thin supported dual layer (*top*) and mixed matrix (*bottom*) membranes prepared via dip-coating and drop-casting methods.

be tuned by either anisotropic crystal growth or thermodynamically limiting the layer stacking [42–44]. The main driving force for the bottom-up synthesis is the diffusion of the metal and ligand sources into the intermediate spacer layer which can be tuned by temperature as reported by Shete *et al.* [45].

Recently, an advancement of free-standing 2D MOF MMMs has been achieved by incorporating the Cu-BDC and $NH_2$-MIL-53(Al) nanosheets in Matrimid® and 6FDA-DAM membranes, showing a significant enhancement of $CO_2/CH_4$ selectivity relative to the pristine membranes [38,39,45,46]. This confirms the role of lamellar morphology of the fillers with high aspect ratio that could facilitate a perpendicular pore orientation and shorter diffusion paths for desired components, while increasing that for undesired components making their permeation pathway more tortuous [47]. More recently, the synthesis of thin 2D MOF MMMs has been reported by Cheng et al. [11].

Here, we report the scaled-up synthesis of Cu-BDC nanosheets and fabrication of free-standing and thin supported membranes comprising these Cu-BDC nanosheets and commercially available PEO-PBT block copolymer (Polyactive™). In order to demonstrate the scope of this approach, the influence of different fabrication methods on the permeation performance of two membrane extremes, viz. thin MMMs with well mixed and DLMs with completely segregated components, was studied in relation to $CO_2$ capture.

## 2. Experimental

### 2.1. Synthesis

#### 2.1.1. Cu-BDC nanosheet scaled-up synthesis

Cu-BDC nanosheets were prepared following the bottom-up route introduced by Rodenas *et al.* [37]. In this study, the nanosheet synthesis was modified and scaled up where the amount of reactants and solvent was multiplied by 50. The linker layer was prepared by dissolving 1.5 g terephthalic acid (Sigma Aldrich, 99%) in a mixture of 100 mL N,N-dimethylformamide (DMF, Sigma Aldrich, > 99%) and 50 mL acetonitrile (Sigma Aldrich, analytical grade) and was added to the 500 mL Duran® bottle as the bottom layer. The intermediate layer (spacer) consisted of 100 mL DMF and 100 mL acetonitrile and was added gently to the bottle. The top layer was prepared by dissolving 1.5 g Cu $(NO_3)_2{\cdot}3H_2O$ (Sigma Aldrich) in a mixture of 100 mL acetonitrile and 50 mL DMF and was added to the bottle without mixing. Then, the bottle was kept in the oven at 40 °C for 24 h. The as-synthesized nanosheets were collected by centrifugation and after removing the supernatant, the solvent were replaced with fresh DMF. This procedure was repeated three times and the next step was using tetrahydrofuran (THF, Sigma Aldrich, > 99%) to centrifuge samples via identical procedure as DMF washing (in this study both chloroform and THF were used for comparison). Finally, the synthesized nanosheets were dispersed in chloroform (Sigma Aldrich, anhydrous) for membrane preparation.

#### 2.1.2. Free-standing MMMs preparation via solution-casting

to fabricate the free-standing membranes, Polyactive™ (Mw ~ 35000 g/mol, Polyvation, NL) granules were degassed for 2 h at 353 K under vacuum and then, 0.2 g dried polymer was dissolved in 2.5 mL chloroform. The proper amount of Cu-BDC nanosheet suspension in chloroform were ultrasonicated for 20 min. Then, 10% of dissolved polymer was added to the suspension and was stirred for 2 h. The rest of the polymer solution was added to the mixture and stirred overnight. The solvent/filler-polymer weight ratio was kept constant (95/5) in all cases. The casting solution was poured on the Teflon petri dish and was covered with a top-drilled box (30.5 cm length × 15.5 cm height × 23.0 cm width) overnight under chloroform-saturated atmosphere. Finally, the membranes were treated under vacuum at 353 K for 24 h. The neat membranes were also prepared with identical approach, without the addition of nanosheets.

#### 2.1.3. Thin supported MMMs preparation via dip-coating

To prepare the thin supported MMMs, polyacrylonitrile (PAN; supplied from AMT® Co. Ltd) porous UF membrane with pore size around 100 nm and $ZrO_2$ coated alumina (supplied from Fraunhofer IKTS, Germany) with pore size around 3 nm were used as support. The dip-coating method was used to coat the supports with the polymer/nanosheet mixture (4 and 8 wt% nanosheet in Polyactive™ solution). The mixture used for dip-coating was prepared in a similar way as for the free-standing membranes. However, the amounts were increased by

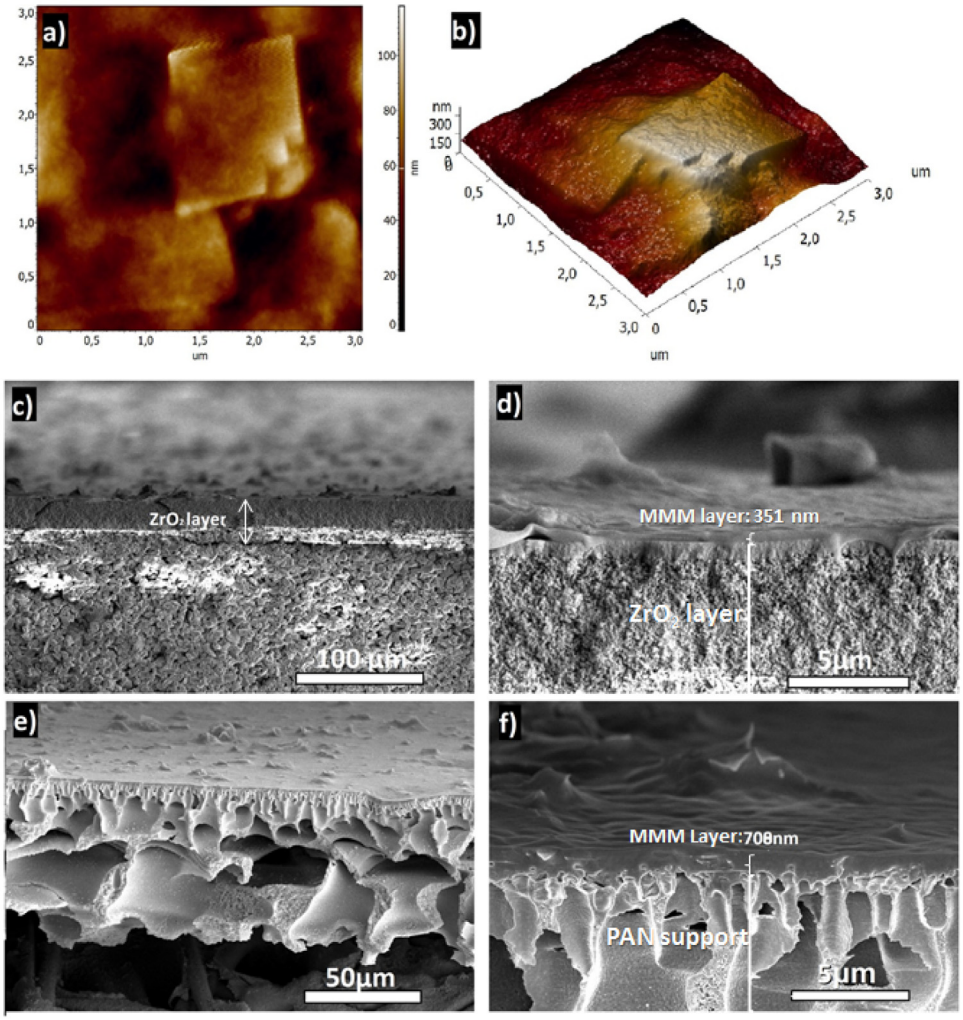


**Fig. 3.** AFM 2D and 3D topography images (a, b) and FE-SEM images of thin MMMs on $ZrO_2$-alumina (c, d) and PAN support (e, f) prepared by dip-coating in the mixture of 8 wt% nanosheet in Polyactive™ (8ns-3PA-MMM).

12 times to prepare the required volume for dip-coating process. The PAN support was pretreated by washing firstly with demi water, and keeping it in the mixture of water and ethanol (50/50) overnight to fill the pores of support. Prior to dip-coating, water droplets were smoothly wiped off from the surface of the support by filter paper. The support was sealed on the Teflon plate by Kapton® tape and was deeply soaked in 3 wt% PDMS in hexane solution (*Sylgard*® 184 Silicone Elastomer). In order to cure the PDMS gutter layer, the support was heat-treated at 100 °C for 30 min. Then, the PDMS coated support was soaked in the polymer/nanosheet mixture vertically and left to dry in a closed Petri dish at room temperature for 24 h. The same procedure was used to prepare the thin membranes on the $ZrO_2$-alumina support. For the sample identification, the *x*ns-*y*PA-PDMS-MMM abbreviation was used where *x* represents the weight percentage of nanosheet based on polymer and *y* refers to the polymer concentration in the coating solution.

#### 2.1.4. Thin supported DLM preparation via drop-casting

To fabricate the thin dual layer membranes (DLM), the PAN support was firstly mounted in the vacuum filtration apparatus and was coated with 1 mL highly diluted Cu-BDC nanosheet suspension (0.05 wt%). After drying, the surface of the nanosheets layer was coated with PDMS for the membranes with gutter layer, as described above. Then, 1 mL Polyactive™ solution (0.25–0.5 wt% in Chloroform) was dropwise added on the PDMS or nanosheet layer and the membranes were dried at room temperature for 24 h. Similarly as above for the sample identification the *x*ns-*y*PA-PDMS-DLM abbreviation was used

### 2.2. Characterization

Transmission electron microscopy (TEM) analysis was carried out using a JEOL JEM-2010 microscope operated at 200 keV. Micrograph acquisition was performed with GATAN Digital Micrograph 1.80.70 software. A few drops of MOF dispersed in chloroform were added on a carbon-coated copper grid and then after drying it was placed on the specimen.

Field emission scanning electron microscopy (FE-SEM) was performed in Nova NanoSEM 450 (Thermo Fisher Scientific) operated at 10 kV. To get the cross section images of the membranes, the samples were immersed and fractured in liquid nitrogen and gold-coated prior to scanning.

Atomic force microscopy (AFM) was performed with a Veeco Multimode Nanoscope 3A microscope operating in tapping mode.

XRD patterns of nanosheets and MMMs were obtained in a Bruker-D8 Advance diffractometer using Co-$K\alpha$ radiation ($\lambda$ = 1.78897 Å, 40 kV, 30 mA). The range of 5–60° of $2\theta$ was scanned using a step size of 0.02° and a scan speed of 0.2 s per step in a continuous scanning mode. The XRD patterns of thin MMMs were obtained by Bruker-D8 Discovery diffractometer and using Cu-$K\alpha$ radiation ($\lambda$ = 1.54059 Å, 40 kV, 30 mA).

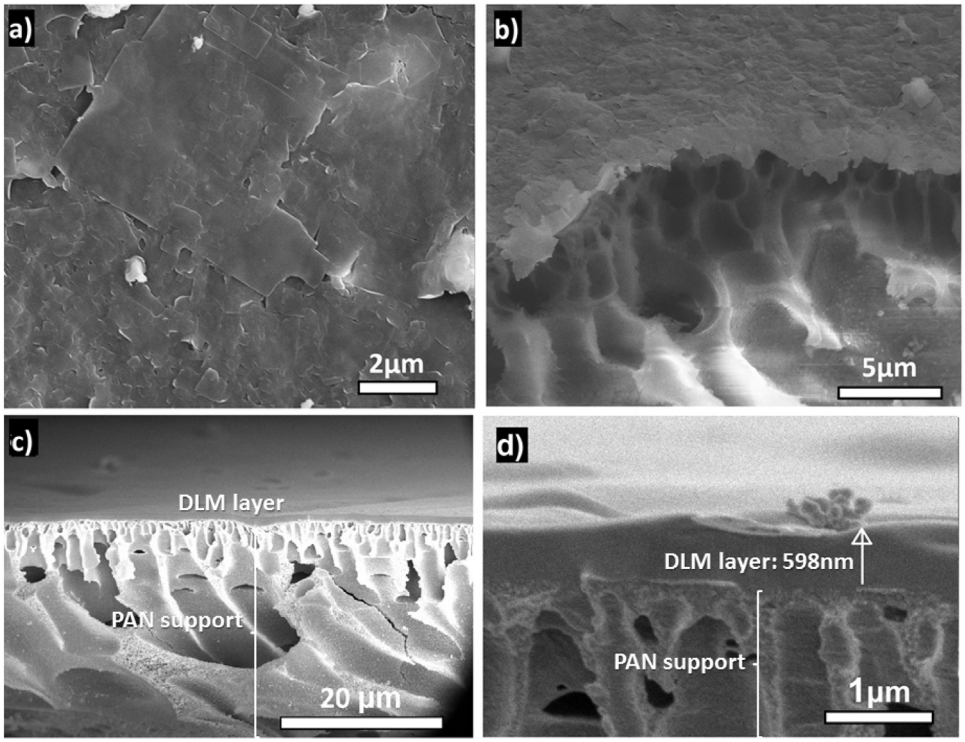


**Fig. 4.** FE-SEM images of surface (a) and cross-section (b) of nanosheets coated on PAN and cross-section images of dual layer thin membranes on PAN prepared by drop-casting (ns-0.25PA-PDMS-DLM) (c, d).

$CO_2$ and $N_2$ adsorption isotherms of Cu-BDC nanosheets were recorded in a Tristar II 3020 (Micromeritics) setup at 273 and 77 K, respectively. Prior to the measurements, the samples were degassed at 423 K under vacuum overnight.

### 2.3. Gas permeation experiments

The separation of $CO_2$ and $N_2$ mixtures at 298 K was conducted in a home-made setup described elsewhere [48]. The membrane samples (area: 1.13 or 3.14 $cm^2$) were prepared and mounted in a flange between two Viton® O-rings. A macroporous stainless steel disc (316 L, 20 μm nominal pore size) was used as support. The permeation module was placed inside a convection oven for controlling the temperature. A mixture (133 mL $min^{-1}$, STP) of $CO_2$ (15 mol.%) and $N_2$ (85 mol.%) flow was used as feed and helium (3 mL $min^{-1}$, STP) was used as a sweep gas. The feed pressure was adjusted to 2 bar (absolute pressure) using a back-pressure controller at the retentate side while the permeate side was kept at atmospheric pressure (1 bar absolute pressure) for all measurements. An online gas chromatograph (Interscience Compact GC) equipped with a packed Carboxen® 1010 PLOT (30 m x 0.32 mm) column and TCD detector was used to analyse the permeate stream.

Gas separation performance was defined by two parameters: the separation factor ($\alpha$, or selectivity) and the gas permeability or permeance. The thin membranes performance mainly defined by permeance which is the pressure normalized flux of the membrane and is reported in Gas Permeation Unit (GPU) where 1 GPU = $1 \times 10^{-6}$ $cm^3$ (STP)/($cm^2$·s·cmHg) or $3.35 \times 10^{-12}$ mol $s^{-1}$ $m^{-2}$ $Pa^{-1}$. The permeance for the component $i$ ($P_i$) was calculated as follows (Eq. (1)):

$$P_i = \frac{F_i}{\Delta p_i \times A} \quad (1)$$

where $F_i$ denotes the molar flow rate of compound $i$, $\Delta p_i$ is the partial pressure difference of $i$ across the membrane, and $A$ is the membrane area.

The separation factor or mixed gas selectivity ($\alpha$) of $CO_2$ over $N_2$ was defined as the ratio of their permeance and can be expressed as follows:

$$\alpha_{CO_2,N_2} = \frac{P_{CO_2}}{P_{N_2}} \quad (2)$$

where $P_{CO_2}$ and $P_{N_2}$ represent the permeance of $CO_2$ and $N_2$, respectively.

## 3. Results and discussion

### 3.1. Characterization scaled-up Cu-BDC nanosheets

Scaled up synthesis of Cu-BDC nanosheet was successfully performed by using the layered route (Fig. 1a) reported by our group [44]. Transmission electron microscopy (TEM) and electron diffraction show the morphology and plane orientation of nanosheets. The equal *d*-spacing of the basal planes in the *xy* direction indicates the tetragonal projection of the crystal structure. (Fig. 1b and c) [45]. Atomic force microscopy (AFM) images of the nanosheets presented in Fig. 1d and e show the square platelet structures with lateral sizes of 1–5 μm and an approximate thickness of 15 nm (Fig. 1e). XRD results of the sample after washing with THF or Chloroform indicate no significant difference in crystallinity. $CO_2$ and $N_2$ adsorption of the scaled-up sample (Fig. 1g, h) show an uptake of $CO_2$ of 0.8 mmol $g^{-1}$ at 1 bar and a BET area of 55 $m^2$ $g^{-1}$. These results are in good agreement with the reported adsorption capacity and BET area of the samples of the original synthesis [39]. The calculated yield of the scaled up synthesis, however, was lower than original synthesis (4% vs. 8%), which might be attributed to the dominant influence of the interfacial area in the three layers approach. Although the amount of reactants was increased up to 50 times, the interface area in scaled-up synthesis was approximately 3.8 times larger than in the original synthesis (Fig. 1a). This confirms the key role of interface area in promoting the yield of reaction by providing the sufficient surface to contact the reactants by diffusional transport.

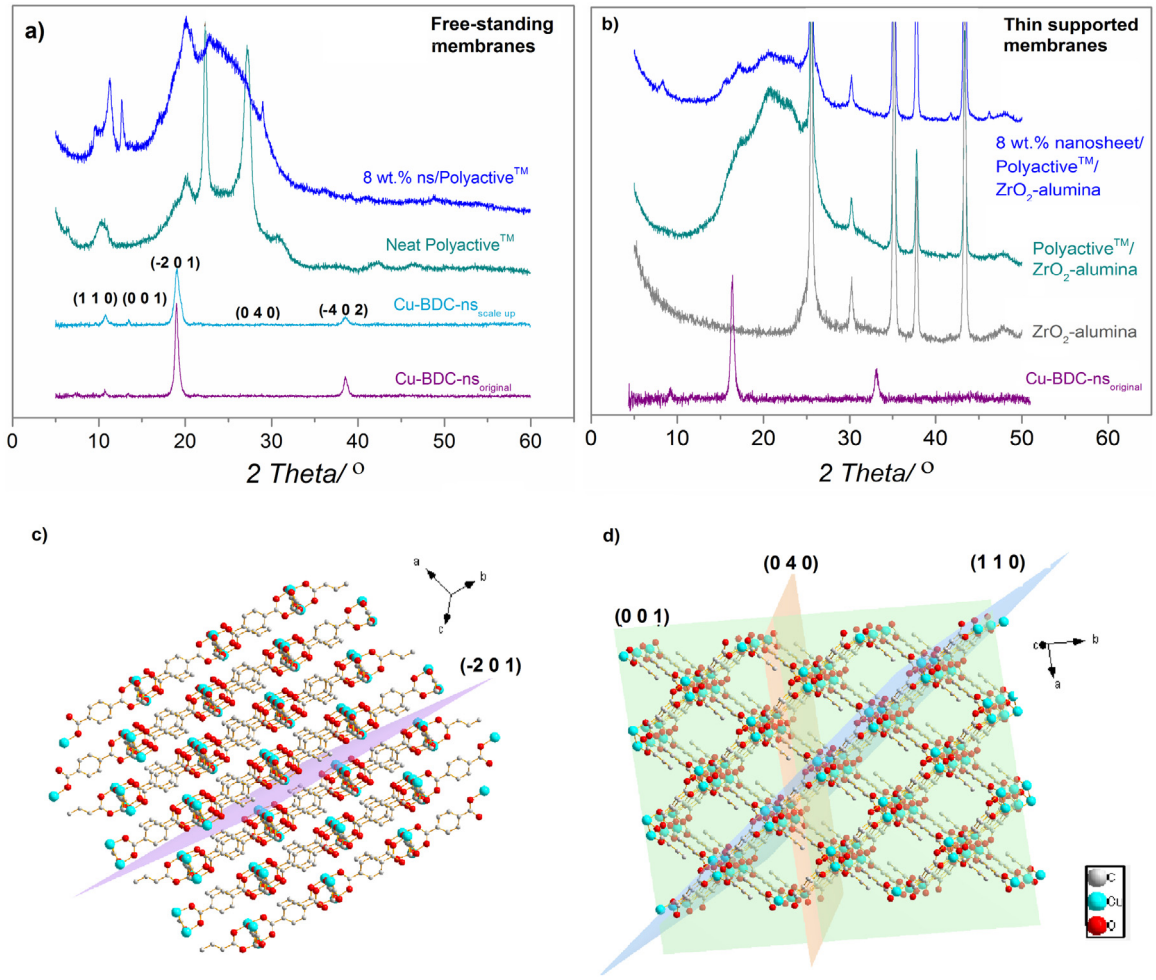


**Fig. 5.** XRD patterns of Cu-BDC nanosheets, free-standing membranes (using Co-*Kα*) (a) and thin membranes (using Cu-*Kα*-radiation) (b), crystal structure of Cu-BDC showing (−2 0 1) (c) and (1 1 0), (0 4 0) and (0 0 1) planes (d).

**Table 1**
Permeation performance of the free-standing MMMs comprising Cu-BDC nanosheets and Polyactive™ at 2 bar and 25 $^{0}$C.

| Membrane | $CO_2$ Permeance (GPU) | $N_2$ Permeance (GPU) | $\alpha_{CO2/N2}$ - | $\delta$ (μm) |
|---|---|---|---|---|
| Neat PA | 3.9 ± 0.2 | 0.07 ± 0.00 | 56 ± 2 | 28 ± 1 |
| 4 wt% ns/PA | 2.6 ± 0.1 | 0.04 ± 0.00 | 59 ± 1 | 37 ± 1 |
| 8 wt% ns/PA | 2.5 ± 0.2 | 0.04 ± 0.00 | 62 ± 0 | 35 ± 1 |
| 16 wt% ns/PA | 3.3 ± 0.2 | 0.05 ± 0.00 | 66 ± 2 | 20 ± 1 |

### 3.2. MMM characterization

Thin supported membranes comprising Cu-BDC nanosheets and Polyactive™ were prepared on porous PAN and $ZrO_2$-alumina supports using two approaches; *i*) Dip-coating and, *ii*) Drop-casting to obtain mixed matrix and dual layer thin membranes, respectively (Fig. 2 & S1).

2D and 3D AFM images of thin MMM (8 ns-3PA; 8 wt% nanosheets in 3 wt% Polyactive™ solution) prepared via dip-coating are shown in Fig. 3a & b. Cross-sectional FE-SEM images of this membrane coated on $ZrO_2$-alumina and PAN supports (without PDMS gutter layer) are shown in Fig. 3c-f. The cross-sectional FE-SEM images reveal that the thin layer formation was successful without polymer penetration in to the finger-like pores of the PAN support, which could be attributed to the fast solvent ($CHCl_3$) evaporation and vertical orientation of membrane during drying (Fig. S1) [49]. Comparing the thin MMMs coated on PAN and on $ZrO_2$-alumina revealed that the thickness was 50% lower in case of $ZrO_2$-alumina support (351 vs. 708 nm) (Fig. 3c & d). This is ascribed to the lower top surface roughness of $ZrO_2$-alumina (pore size ~3 nm) and less adherence of coating solution to the support.

In contrast, using drop-casting resulted in a smooth surface of the thin membranes, representing horizontally aligned nanosheets by vacuum filtration on the support (Fig. 4a & b) and an adequate coverage of the nanosheets by the polymer layer (Fig. 4c & d).

XRD patterns of Cu-BDC nanosheets and free-standing membranes are compared in Fig. 5a. Polyactive™ neat membrane shows a certain degree of crystallinity [50]. However, by addition of Cu-BDC nanosheets into Polyactive™, the reflections of the polymer that appeared in the range of $2\Theta$ ~22–27° became wider and overlapped (Fig. 5a). Moreover, the polymer reflection slightly shifted to higher $2\Theta$ (lower *d*-spacing), showing reduction in polymer chains spacing as was previously reported by Zornoza et al. [48,51]. Further, the typical reflections of Cu-BDC nanosheets which were indexed as (−2 0 1) and (−4 0 2) shifted slightly and their intensity decreased. In turn, the reflections of the (1 1 0), (0 4 0) planes (Fig. 5c & d), are more visible in the MMMs. These results indicate a change in the orientation of the nanosheets in free-standing MMMs which might have arisen from shear forces during membrane preparation and solvent evaporation [11,52]. In contrast, thin supported neat Polyactive™ membranes and the relevant thin MMMs showed different patterns as indicated in Fig. 5b. This might be attributed to the ultrafast drying of the thin layer during the dip-coating process, changing the polymer chain packing and resulting in broadened reflections of thin supported membranes compared to free-standing membranes. The addition of nanosheets to the

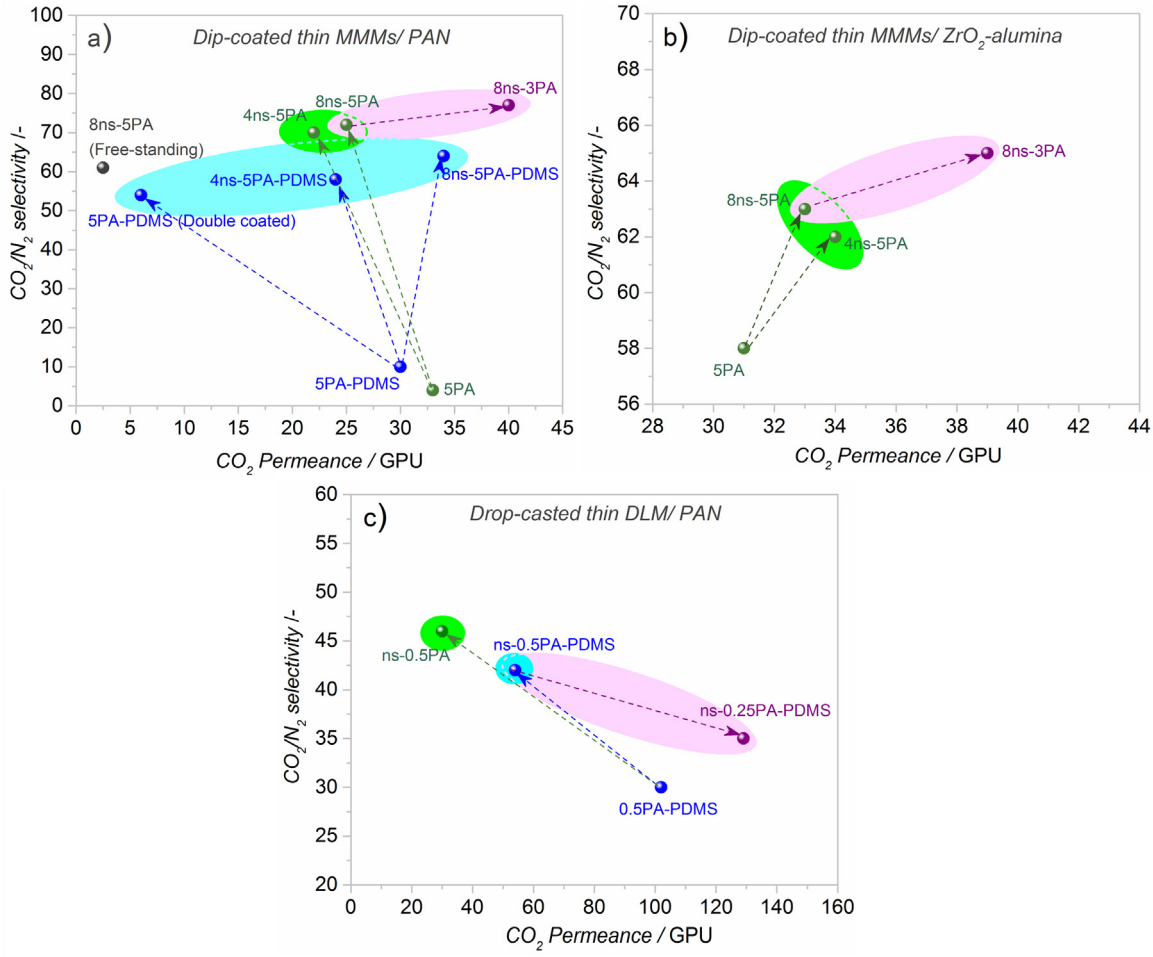


**Fig. 6.** $CO_2$ and $N_2$ separation performance of dip-coated thin MMMs on (a) PAN, and (b) $ZrO_2$-alumina support, (c) thin dual layer membranes drop-casted on PAN support at 298 K and 2 bar absolute feed pressure (mixed gases). In the sample identification *x* represents the weight percent of nanosheets based on polymer and *y* refers to the polymer concentration in the coating solution.

**Table 2**
Separation performance of MOF based thin supported and asymmetric MMMs reported in literature and the comparison with this study.

| Thin MMMs | Feed conditions *p*(bar), *T*(°C) | Feed gas $CO_2/N_2$ ratio | $CO_2$ Permeance (GPU) | $\alpha_{CO2/N2}$ - | Data no.[c] | Ref |
|---|---|---|---|---|---|---|
| Cu-MOF/POZ (1500 nm) | 2, 25 | Single gas | 6 | 30 | 12 | [57] |
| Cu-BTC/Matrimid (asymmetric) | 5, 35 | 35/65 | 19 | 23 | 13 | [58] |
| Cu-MOF/Pebax (1500 nm) | 2, 25 | Single gas | 14 | 47 | 14 | [59] |
| MIL-53/Matrimid (asymmetric) | 5, 35 | 35/65 | 21 | 24 | 15 | [58] |
| ZIF-8/Matrimid (asymmetric) | 5, 35 | 35/65 | 20 | 20 | 16 | [58] |
| S-MIL-53/Ultem(asymmetric) | 5, 25 | Single gas | 24 | 41 | 17 | [60] |
| ZIF-7/ Pebax (500 nm) | 3.5, 25 | Single gas | 291 | 67 | 19 | [61] |
| Dual layer Cu-BDC/Polyactive (600 nm)[a] | 2, 25 | 15/85 | 129 | 35 | 11 | This study |
| MMM Cu-BDC/Polyactive (700 nm)[b] | 2, 25 | 15/85 | 40 | 77 | 7 | This study |

[a] With PDMS as gutter layer on PAN support (ns-0.25PA-PDMS).
[b] Without PDMS as gutter layer on PAN support (8ns-3PA).
[c] Data number refers to Fig. 7.

polymer slightly changed the crystallinity of the neat membrane and the nanosheet reflections corresponding to (−2 0 1) and (1 1 0) planes with direction toward pore accessibility were observed. However, the reflections attributed to (0 0 1), (0 4 0) and (−4 0 2) planes were not strong enough which might be due to the less loading of nanosheets or different orientation in the thin membranes.

### 3.3. Gas separation performance

The free-standing membranes fabricated by solution casting were tested under identical condition as reported previously [30]. Table 1 shows their $CO_2$ and $N_2$ separation performance parameters. The increase in nanosheet loading (from 0 to 16 wt%) resulted in a monotonous improvement in selectivity (from 56 to 66) along with a decrease of gas permeance. The obtained permeation results are in good agreement with reported data of MMMs using Cu-BDC nanosheets with Matrimid® or 6FDA-DAM as the continuous matrix [39,45,46]. The decrease in permeance of the MMMs is in line with XRD patterns of the free-standing membranes, showing reduction in polymer chains distance and a partial change in orientation of nanosheets towards non-

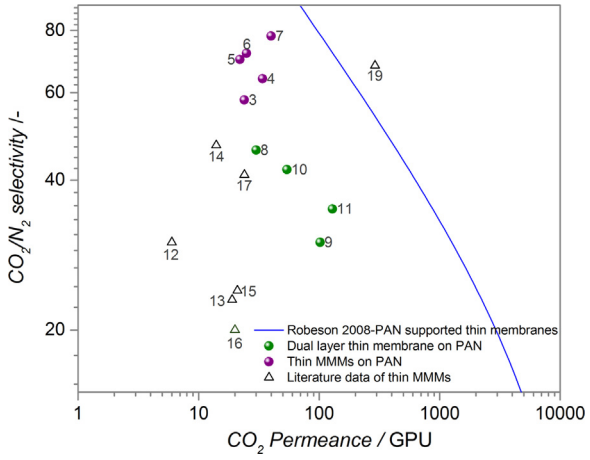


**Fig. 7.** Effective Robeson limit of $CO_2$ / $N_2$ separation performance of PAN supported thin membranes (*blue line*, calculation in SI) and the comparison of thin supported MMMs (*purple circles*) and dual layer membranes (*green circles*) at 298 K and 2 bar absolute feed pressure ($CO_2/N_2$ mixed gases 15/85 by volume). Experimental and literature data of MOF-based thin supported and asymmetric MMMs are shown for comparison and listed in Table 2 (*open symbols*) and Table S1 (*closed symbols*). (For interpretation of the references to color in this figure legend, the reader is referred to the web version of this article.).

accessible porosity of MOF in MMMs. Further, the flexible polymer chains might penetrate into pores of the nanosheets and partially block the porosity of MOF [50].

The thin membranes prepared by two different approaches (dip-coating and drop-casting methods) were tested under identical conditions as for the free-standing membranes. The permeation results of thin supported MMMs prepared by dip-coating with and without using PDMS as gutter layer are presented in Fig. 6a. The selectivity of the neat thin membrane was very low (~ 10) which could be attributed to the large pore size of the PAN support and defect formation. Coating with a PDMS gutter layer improved slightly the selectivity. In order to fabricate a thin neat Polyactive™ membrane with expected intrinsic selectivity, a double coating approach was applied. However, a considerable drop in $CO_2$ permeance to ~ 6 GPU resulted (still above the free standing sample) along with an increase in selectivity to 54, similar as for the pure Polyactive™ membrane. For thin MMMs prepared under identical conditions with single coating, an increase in selectivity (ranging from 58 to 72) was achieved even with an improvement of permeance. The performance of thin MMMs prepared with PDMS gutter layer was only slightly different from the membranes without gutter layer. Therefore, high aspect ratio fillers (nanosheets) could make the PDMS gutter layer and its optimization superfluous with the advantage of obtaining higher selectivity.[1,53] Interestingly, using a lower concentration of polymer solution (3 wt%) resulted in certain improvement in permeance of the thin MMM (to ~ 40 GPU) and increasing the selectivity up to 77 (Fig. 6a; purple symbol). The selectivity is even higher than the optimized free standing MMM (Table 1) which might be attributed to the different polymer chains packing and nanosheet orientation as revealed by XRD studies [11].

To investigate the role of support properties, $ZrO_2$-alumina with much smaller pore size (~ 3 nm) was used to prepare thin membranes via dip-coating (Fig. 6b). The neat thin Polyactive™ membrane without PDMS gutter layer was apparently defect-free showing higher selectivity and permeance than the PAN supported membrane. The thin MMMs coated on $ZrO_2$-alumina showed a simultaneous improvement in permeance and in selectivity, whereas the relevant PAN supported thin MMMs (without PDMS gutter layer) only showed improvement in selectivity and decrease in permeance. The thin MMMs coated on PAN, however, showed a higher selectivity using the same formulation, which might be attributed to the influence of support resistance on selectivity by Knudsen diffusion as reported by Kattula et al. for polymeric membranes [1,53] and by Kapteijn et al. for zeolite membranes [54]. Decreasing the polymer concentration from 5 to 3 wt% in the $ZrO_2$-alumina supported thin MMMs resulted in a further increase in permeance to ~ 40 GPU while selectivity hardly changed (65) (Fig. 6b; purple symbol). Considering the thickness, the FE-SEM images (Fig. S2) showed a 50–60% reduction in the thickness of the thin membranes. The same dilution for the PAN supported membranes resulted in an improvement of permeance from 25 to 40 GPU and selectivity from 72 to 77. This higher selectivity is attributed to the lower resistance of the PAN support compared to the small pore size $ZrO_2$-alumina support [1,55]. Finally, 3 wt% was found the lower limit for diluting the polymer concentration using dip-coating; at lower concentrations no defect-free thin film was obtained.

To utilize the morphological advantages of high aspect ratio nanosheets more efficiently in thin film formation, thin PAN-supported dual layer membranes (DLMs) were prepared by drop-casting (Fig. 2). Their permeation properties are indicated in Fig. 6c. The higher permeance of the thin DLMs than MMMs confirms that the polymer chains packing and the orientation of the nanosheets were not influenced. However, the selectivity of the dip-coated thin MMMs was higher than the thin DLMs, which signifies the role of spatial distribution of nanosheets and the polymer chains distance on the selectivity in thin MMMs [56]. A PDMS gutter layer had a more pronounced influence on the permeation performance of thin dual layer membranes. The permeance with a PDMS gutter layer was 66% higher than without PDMS while the selectivity did not change significantly (Fig. 6c; blue & green arrows). Decreasing the Polyactive™ concentration in the drop-casting solution from 0.5 to 0.25 wt% further improved the permeance (2.5 times) of the thin membranes while selectivity was slightly decreased (16%). As a result, it can be concluded that preparing thin dual layer membranes via drop-casting is promising in terms of permeance. However, the spatial distribution of nanosheets, like in MMMs, is an essential parameter to effectively improve the selectivity of the thin membranes.

Comparison with reported MOF based thin supported and asymmetric MMMs, the thin membranes in this study showed a superior $CO_2/N_2$ separation performance when utilizing high aspect ratio nanosheets, even in combination with a selective polymer (Table 2). The selectivity of the studied membranes exceeded most of the reported values of MOF based thin MMMs. Although different types of MOF fillers were incorporated in the glassy and rubbery polymer matrix, the results show that by using small pore size ZIFs and high aspect ratio nanosheets in rubbery polymers the selectivity can be enhanced. This is attributed to the defect covering properties of the nanosheets and their perpendicular orientation towards gas permeation when homogeneously dispersed in the MMM. For the other extreme, the fully segregated polymer and nanosheet layers in the dual layer membrane, their permeance was promising in comparison with most reported thin MOF-based MMMs, although the selectivity was lower than for the homogeneous MMM. (Fig. 7).

## 4. Conclusions

In summary, utilizing Cu-BDC nanosheets prepared in a scaled-up synthesis and the selective Polyactive™ polymer to fabricate supported thin MMMs and DLMs was demonstrated to results in membranes with improved separation performance. The main role of nanosheets was found to cover the defects during the thin membrane formation, making a gutter layer superfluous, and improving the $CO_2/N_2$ selectivity of the thin membranes up to 77.

Mixed matrix and dual-layer thin membranes of Cu-BDC nanosheets and polymer, prepared via dip-coating and drop-casting, were compared as two extreme systems with homogeneously mixed or completely segregated components for their separation performance. Using Cu-BDC nanosheets well dispersed in thin supported mixed matrix

membranes significantly improved the selectivity, even higher than identical free-standing membranes (77 vs. 60), and the $CO_2$ permeance to 40 GPU.

Comparison of PAN and $ZrO_2$-alumina as supports shows that pore size, porosity and roughness affect the obtained separation layer thickness and their resistance can negatively affect the $CO_2/N_2$ selectivity. The findings in this study are relevant in development of optimized preparation methods of defect-free thin supported MMMs.

## Acknowledgments

The research leading to these results has received funding from the European Union Seventh Framework Programme (*FP7/2007–2013*) under *grant agreement* n° 608490.

## Appendix A. Supplementary material

Supplementary data associated with this article can be found in the online version at doi:10.1016/j.memsci.2018.10.047.

## References

[1] H.B. Park, J. Kamcev, L.M. Robeson, M. Elimelech, B.D. Freeman, Maximizing the right stuff: the trade-off between membrane permeability and selectivity, Science 356 (2017) 1–10.
[2] X. He, Membranes for natural gas sweetening, in: E. Drioli, L. Giorno (Eds.), Encyclopedia of Membranes, Springer Berlin Heidelberg, Berlin, Heidelberg, 2016, pp. 1266–1267.
[3] C.A. Scholes, M.T. Ho, A.A. Aguiar, D.E. Wiley, G.W. Stevens, S.E. Kentish, Membrane gas separation processes for $CO_2$ capture from cement kiln flue gas, Int. J. Greenh. Gas. Control 24 (2014) 78–86.
[4] E. Sjöberg, L. Sandström, O.G.W. Öhrman, J. Hedlund, Separation of $CO_2$ from black liquor derived syngas using an MFI membrane, J. Membr. Sci. 443 (2013) 131–137.
[5] J.M.S. Henis, M.K. Tripodi, The developing technology of gas separating membranes, Science 220 (1983) 11–17.
[6] R.W. Baker, Membrane Technology and Application, second ed., John Wiley & Sons.Ltd, 2004.
[7] H. Strathmann, P. Scheible, R.W. Baker, A rationale for the preparation of Loeb-Sourirajan-type cellulose acetate membranes, J. Appl. Polym. Sci. 15 (1971) 811–828.
[8] W.J. Lau, A.F. Ismail, N. Misdan, M.A. Kassim, A recent progress in thin film composite membrane: a review, Desalination 287 (2012) 190–199.
[9] Y. Shen, H. Wang, X. Zhang, Y. Zhang, MoS2 nanosheets functionalized composite mixed matrix membrane for enhanced $CO_2$ capture via surface drop-coating method, ACS Appl. Mater. Interfaces 8 (2016) 23371–23378.
[10] M. Karunakaran, R. Shevate, M. Kumar, K.V. Peinemann, $CO_2$-selective PEO-PBT (PolyActive[trade mark sign])/graphene oxide composite membranes, Chem. Commun. 51 (2015) 14187–14190.
[11] Y. Cheng, X. Wang, C. Jia, Y. Wang, L. Zhai, Q. Wang, D. Zhao, Ultrathin mixed matrix membranes containing two-dimensional metal-organic framework nanosheets for efficient $CO_2$/CH4 separation, J. Membr. Sci. 539 (2017) 213–223.
[12] J. Peter, K.V. Peinemann, Multilayer composite membranes for gas separation based on crosslinked PTMSP gutter layer and partially crosslinked Matrimid® 5218 selective layer, J. Membr. Sci. 340 (2009) 62–72.
[13] L. Liu, W.L. Qiu, E.S. Sanders, C.H. Ma, W.J. Koros, Post-combustion carbon dioxide capture via 6FDA/BPDA-DAM hollow fiber membranes at sub-ambient temperatures, J. Membr. Sci. 510 (2016) 447–454.
[14] H.Q. Lin, Z.J. He, Z. Sun, J.M. Vu, A. Ng, M. Mohammed, J. Kniep, T.C. Merkel, T. Wu, R.C. Lambrecht, $CO_2$-selective membranes for hydrogen production and $CO_2$ capture - Part I: membrane development, J. Membr. Sci. 457 (2014) 149–161.
[15] L.S. White, K.D. Amo, T. Wu, T.C. Merkel, Extended field trials of Polaris sweep modules for carbon capture, J. Membr. Sci. 542 (2017) 217–225.
[16] R.W. Baker, J.G. Wijmans, T.C. Merkel, H. Lin, R. Daniels, S. Thompson, Gas separation process using membranes with permeate sweep to remove CO2 from combustion gases, in: US Patent, Membrane Technology and Research Inc., US, 2008.
[17] X. He, The latest development on membrane materials and processes for post-combustion $CO_2$ capture: a review, SF J. Mater. Chem. Eng. 1 (2018) 1009–1018.
[18] P. Bernardo, E. Drioli, G. Golemme, Membrane gas separation: a review/state of the art, Ind. Eng. Chem. Res. 48 (2009) 4638–4663.
[19] T.T. Moore, W.J. Koros, Non-ideal effects in organic–inorganic materials for gas separation membranes, J. Mol. Struct. 739 (2005) 87–98.
[20] Z. Dai, L. Ansaloni, L. Deng, Recent advances in multi-layer composite polymeric membranes for $CO_2$ separation: a review, Green Energy Environ. 1 (2016) 102–128.
[21] A. Sabetghadam, X. Liu, M. Benzaqui, E. Gkaniatsou, A. Orsi, M.M. Lozinska, C. Sicard, T. Johnson, N. Steunou, P.A. Wright, C. Serre, J. Gascon, F. Kapteijn, Influence of filler pore structure and polymer on the performance of MOF-based mixed-matrix membranes for $CO_2$ capture, Chem. – Eur. J. 24 (2018) 7949–7956.
[22] S. Zhao, X. Cao, Z. Ma, Z. Wang, Z. Qiao, J. Wang, S. Wang, Mixed-matrix membranes for $CO_2$/N2 separation comprising a poly(vinylamine) matrix and metal–organic frameworks, Ind. Eng. Chem. Res 54 (2015) 5139–5148.
[23] Y. Chen, L. Zhao, B. Wang, P. Dutta, W.S. Winston Ho, Amine-containing polymer/zeolite Y composite membranes for $CO_2$/N2 separation, J. Membr. Sci. 497 (2016) 21–28.
[24] A. Halim, Q. Fu, Q. Yong, P.A. Gurr, S.E. Kentish, G.G. Qiao, Soft polymeric nanoparticle additives for next generation gas separation membranes, J. Mater. Chem. A 2 (2014) 4999–5009.
[25] C. Zou, Q. Li, Y. Hua, B. Zhou, J. Duan, W. Jin, Mechanical synthesis of COF nanosheet cluster and its mixed matrix membrane for efficient $CO_2$ removal, ACS Appl. Mater. Interfaces 9 (2017) 29093–29100.
[26] Y. Ban, Y. Li, Y. Peng, H. Jin, W. Jiao, X. Liu, W. Yang, Metal-substituted Zeolitic imidazolate framework ZIF-108: gas-sorption and membrane-separation properties, Chem. – Eur. J. 20 (2014) 11402–11409.
[27] T. Brinkmann, C. Naderipour, J. Pohlmann, J. Wind, T. Wolff, E. Esche, D. Müller, G. Wozny, B. Hoting, Pilot scale investigations of the removal of carbon dioxide from hydrocarbon gas streams using poly (ethylene oxide)–poly (butylene terephthalate) PolyActive™) thin film composite membranes, J. Membr. Sci. 489 (2015) 237–247.
[28] W. Yave, A. Car, J. Wind, K.-V. Peinemann, Nanometric thin film membranes manufactured on square meter scale: ultra-thin films for CO 2 capture, Nanotechnology 21 (2010) 395301–395308.
[29] M. Etxeberria-Benavides, O. David, T. Johnson, M.M. Łozińska, A. Orsi, P.A. Wright, S. Mastel, R. Hillenbrand, F. Kapteijn, J. Gascon, High performance mixed matrix membranes (MMMs) composed of ZIF-94 filler and 6FDA-DAM polymer, J. Membr. Sci. 550 (2018) 198–207.
[30] A. Sabetghadam, X. Liu, A.F. Orsi, M.M. Lozinska, T. Johnson, K.M.B. Jansen, P.A. Wright, M. Carta, N.B. McKeown, F. Kapteijn, J. Gascon, Towards high performance metal–organic framework–microporous polymer mixed matrix membranes: addressing compatibility and limiting aging by polymer doping, Chem. – Eur. J. 24 (2018) 12796–12800.
[31] M.H.-O. Rashid, S.F. Ralph, Carbon nanotube membranes: synthesis, properties, and future filtration applications, Nanomaterials 7 (2017) 99–127.
[32] R.K. Joshi, S. Alwarappan, M. Yoshimura, V. Sahajwalla, Y. Nishina, Graphene oxide: the new membrane material, Appl. Mater. Today 1 (2015) 1–12.
[33] Z. Han, X. Qiang, G. Xianghai, L. Najun, K. Prashant, R. Neel, J.M. Young, A.-T. Shaeel, N. Katabathini, B.S. Nasir, T. Berna, O.F. J, M.C. W, M.K. Andre, T. Michael, Open-pore two-dimensional MFI zeolite nanosheets for the fabrication of hydrocarbon-isomer-selective membranes on porous polymer supports, Angew. Chem. Int. Ed. 55 (2016) 7184–7187.
[34] Y. Peng, Y. Li, Y. Ban, H. Jin, W. Jiao, X. Liu, W. Yang, Metal-organic framework nanosheets as building blocks for molecular sieving membranes, Science 346 (2014) 1356–1359.
[35] K. Varoon, X. Zhang, B. Elyassi, D.D. Brewer, M. Gettel, S. Kumar, J.A. Lee, S. Maheshwari, A. Mittal, C.-Y. Sung, M. Cococcioni, L.F. Francis, A.V. McCormick, K.A. Mkhoyan, M. Tsapatsis, Dispersible exfoliated zeolite nanosheets and their application as a selective membrane, Science 334 (2011) 72–75.
[36] C. Sunho, C. Joaquin, J. Edgar, O. Weontae, N. Sankar, O. Frank, S.D. F, T. Michael, Layered silicates by swelling of AMH-3 and nanocomposite membranes, Angew. Chem. Int. Ed. 47 (2008) 552–555.
[37] A. Sabetghadam, B. Seoane, D. Keskin, N. Duim, T. Rodenas, S. Shahid, S. Sorribas, C.L. Guillouzer, G. Clet, C. Tellez, M. Daturi, J. Coronas, F. Kapteijn, J. Gascon, Metal organic framework crystals in mixed-matrix membranes: impact of the filler morphology on the gas separation performance, Adv. Funct. Mater. 26 (2016) 3154–3163.
[38] A. Pustovarenko, M.G. Goesten, S. Sachdeva, M. Shan, Z. Amghouz, Y. Belmabkhout, A. Dikhtiarenko, T. Rodenas, D. Keskin, I.K. Voets, B.M. Weckhuysen, M. Eddaoudi, L.C.P.M. de Smet, E.J.R. Sudhölter, F. Kapteijn, B. Seoane, J. Gascon, Nanosheets of nonlayered aluminum metal–organic frameworks through a surfactant-assisted method, Adv. Mater. 30 (2018) 1707234–1707242.
[39] T. Rodenas, I. Luz, G. Prieto, B. Seoane, H. Miro, A. Corma, F. Kapteijn, I.X.F.X. Llabres, J. Gascon, Metal-organic framework nanosheets in polymer composite materials for gas separation, Nat. Mater. 14 (2015) 48–55.
[40] A. Corma, V. Fornes, S.B. Pergher, T.L.M. Maesen, J.G. Buglass, Delaminated zeolite precursors as selective acidic catalysts, Nature 396 (1998) 353–356.
[41] Y. Hernandez, V. Nicolosi, M. Lotya, F.M. Blighe, Z. Sun, S. De, I.T. McGovern, B. Holland, M. Byrne, Y.K. Gun'Ko, J.J. Boland, P. Niraj, G. Duesberg, S. Krishnamurthy, R. Goodhue, J. Hutchison, V. Scardaci, A.C. Ferrari, J.N. Coleman, High-yield production of graphene by liquid-phase exfoliation of graphite, Nat. Nanotechnol. 3 (2008) 563–568.
[42] M. Choi, K. Na, J. Kim, Y. Sakamoto, O. Terasaki, R. Ryoo, Stable single-unit-cell nanosheets of zeolite MFI as active and long-lived catalysts, Nature 461 (2009) 246–249.
[43] G. Hu, N. Wang, D. O'Hare, J. Davis, One-step synthesis and AFM imaging of hydrophobic LDH monolayers, Chem. Commun. (2006) 287–289.
[44] T. Rodenas, M. van Dalen, P. Serra-Crespo, F. Kapteijn, J. Gascon, Mixed matrix membranes based on NH2-functionalized MIL-type MOFs: influence of structural and operational parameters on the $CO_2$/CH4 separation performance, Microporous Mesoporous Mater. 192 (2014) 35–42.
[45] M. Shete, P. Kumar, J.E. Bachman, X. Ma, Z.P. Smith, W. Xu, K.A. Mkhoyan, J.R. Long, M. Tsapatsis, On the direct synthesis of Cu(BDC) MOF nanosheets and their performance in mixed matrix membranes, J. Membr. Sci. 549 (2018) 312–320.
[46] Y. Yang, K. Goh, R. Wang, T.-H. Bae, High-performance nanocomposite membranes realized by efficient molecular sieving with CuBDC nanosheets, Chem. Commun. 53

(2017) 4254–4257.
[47] X. Li, Y. Cheng, H. Zhang, S. Wang, Z. Jiang, R. Guo, H. Wu, Efficient $CO_2$ capture by functionalized graphene oxide nanosheets as fillers to fabricate multi-permselective mixed matrix membranes, ACS Appl. Mater. Interfaces 7 (2015) 5528–5537.
[48] B. Zornoza, A. Martinez-Joaristi, P. Serra-Crespo, C. Tellez, J. Coronas, J. Gascon, F. Kapteijn, Functionalized flexible MOFs as fillers in mixed matrix membranes for highly selective separation of $CO_2$ from CH4 at elevated pressures, Chem. Commun. 47 (2011) 9522–9524.
[49] D. Grosso, How to exploit the full potential of the dip-coating process to better control film formation, J. Mater. Chem. 21 (2011) 17033–17038.
[50] M. Shan, B. Seoane, E. Andres-Garcia, F. Kapteijn, J. Gascon, Mixed-matrix membranes containing an azine-linked covalent organic framework: influence of the polymeric matrix on post-combustion $CO_2$-capture, J. Membr. Sci. 549 (2018) 377–384.
[51] L. Ma, F. Svec, T. Tan, Y. Lv, Mixed matrix membrane based on cross-linked poly [(ethylene glycol) methacrylate] and metal–organic framework for efficient separation of carbon dioxide and methane, ACS Appl. Nano Mater. 1 (2018) 2808–2818.
[52] X. Wang, C. Chi, K. Zhang, Y. Qian, K.M. Gupta, Z. Kang, J. Jiang, D. Zhao, Reversed thermo-switchable molecular sieving membranes composed of two-dimensional metal-organic nanosheets for gas separation, Nat. Commun. 8 (2017) 14460–14470.
[53] M. Kattula, K. Ponnuru, L. Zhu, W. Jia, H. Lin, E.P. Furlani, Designing ultrathin film composite membranes: the impact of a gutter layer, Sci. Rep. 5 (2015) 15016–15025.
[54] W.Z.F. Kapteijn, J.A. Moulijn, T.Q. Gardner, Zeolite membranes: modeling and application, in: J.A.M.A. Cybulski (Ed.), Structured Catalysts and Reactors, CRC Taylor & Francis, USA, 2006, pp. 700–746.
[55] F.T. de Bruijn, L. Sun, Ž. Olujić, P.J. Jansens, F. Kapteijn, Influence of the support layer on the flux limitation in pervaporation, J. Membr. Sci. 223 (2003) 141–156.
[56] T. Rodenas, Mv Dalen, E. García-Pérez, P. Serra-Crespo, B. Zornoza, F. Kapteijn, J. Gascon, Visualizing MOF mixed matrix membranes at the nanoscale: towards structure-performance relationships in $CO_2$/CH4 separation Over NH2-MIL-53(Al) @PI, Adv. Funct. Mater. 24 (2014) 249–256.
[57] S.Y. Lim, J. Choi, H.-Y. Kim, Y. Kim, S.-J. Kim, Y.S. Kang, J. Won, New $CO_2$ separation membranes containing gas-selective Cu-MOFs, J. Membr. Sci. 467 (2014) 67–72.
[58] S. Basu, A. Cano-Odena, I.F.J. Vankelecom, MOF-containing mixed-matrix membranes for $CO_2$/CH4 and $CO_2$/N2 binary gas mixture separations, Sep. Purif. Technol. 81 (2011) 31–40.
[59] J. Kim, J. Choi, Y. Soo Kang, J. Won, Matrix effect of mixed-matrix membrane containing $CO_2$-selective MOFs, J. Appl. Polym. Sci. 133 (2016) 42853–42861.
[60] H. Zhu, L. Wang, X. Jie, D. Liu, Y. Cao, Improved interfacial affinity and $CO_2$ separation performance of asymmetric mixed matrix membranes by incorporating postmodified MIL-53(Al), ACS Appl. Mater. Interfaces 8 (2016) 22696–22704.
[61] T. Li, Y. Pan, K.-V. Peinemann, Z. Lai, Carbon dioxide selective mixed matrix composite membrane containing ZIF-7 nano-fillers, J. Membr. Sci., 425- 426 (2013) 235–242.